Multiple Kronecker RLS fusion-based link propagation for drug-side effect prediction

Anonymous authors
Paper under double-blind review

Abstract

Drug-side effect prediction has become an essential area of research in the field of pharmacology. As the use of medications continues to rise, so does the importance of understanding and mitigating the potential risks associated with them. At present, researchers have turned to data-driven methods to predict drug-side effects. Drug-side effect prediction is a link prediction problem, and the related data can be described from various perspectives. To process these kinds of data, a multi-view method, called Multiple Kronecker RLS fusion-based link propagation (MKronRLSF-LP), is proposed. MKronRLSF-LP extends the Kron-RLS by finding the consensus partitions and multiple graph Laplacian constraints in the multi-view setting. Both of these multi-view settings contribute to a higher quality result. Extensive experiments have been conducted on drug-side effect datasets, and our empirical results provide evidence that our approach is effective and robust.

1 Introduction

Pharmacovigilance is critical to drug safety and surveillance. The field of pharmacovigilance plays a crucial role in public health by continuously monitoring and evaluating the safety profile of drugs. Pharmacovigilance involves collecting and analyzing data from various sources, including health care professionals Yang et al. (2016), patients, regulatory authorities, and pharmaceutical companies. These data are then used to identify possible side effects and assess their severity and frequency Da Silva & Krishnamurthy (2016); Galeano et al. (2020). Traditionally, drug-side effects were primarily identified through spontaneous reporting systems, where health care professionals and patients reported adverse events to regulatory authorities. However, this approach has limitations, such as underreporting and delayed detection.

To overcome these limitations, researchers have turned to data-driven methods to find drug-side effects. With the advent of electronic health records, large-scale databases containing valuable information on medication usage and patient outcomes have become available. These databases have allowed researchers to analyze vast amounts of data to identify patterns between drugs and side effects.

One of the most commonly used approaches in drug-side effects prediction is model-based methods. Model-based methods involve the use of advanced statistical and machine learning techniques to extract knowledge from large datasets. By analyzing patterns in the data, researchers can identify potential drug-side effects and their associated risk factors. In their work, Pauwels et al. Pauwels et al. (2011) predicted the side effects of drugs by applying K-nearest neighbor (KNN), support vector machine (SVM), ordinary canonical correlation analysis (OCCA) and sparse canonical correlation analysis (SCCA) from drug chemical substructures; furthermore, their experiment outcome suggest that SCCA performs the best. Mizutani et al. Sayaka et al. (2012) utilized SCCA to associate targeted proteins with side effects. A machine learning methodology was presented to predict side effects from the chemical structure, target protein Li et al. (2021) and drug pathway, and they applied SVM, KNN, random forest, logistic regression and naive Bayes to predict side effects. SVM performed the best. Cheng et al. Cheng et al. (2013) proposed a phenotypic network inference classifier to associate drugs with side effects. In Zhang et al. Zhang et al. (2016), an ensemble model based on Liu et al.'s Liu et al. (2012) method, Cheng et al.'s method, the integrated neighbour-based method (INBM)

and restricted Boltzmann machines (RBM) was provided. The authors found that their ensemble method achieved the highest classification accuracy.

Deep learning techniques Xu et al. (2022) have been increasingly used to predict drug side effects in recent years. These methods leverage the power of neural networks to analyze complex relationships between drugs, genes, and proteins. In SDPred Zhao et al. (2022), chemical-chemical associations, chemical substructure, drug target information, word representations of drug molecular substructures, semantic similarity of side effects, and drug side effect associations are integrated. To learn drug-side effect pair representation vectors from different interaction maps, SDPred uses the CNN module. Drug interaction profile similarity (DIPA) provided the most contribution. GCRS Xuan et al. (2022) builds a complex deep-learning structure to fuse and learn the specific topologies, common topologies and pairwise attributes from multiple drug-side effect heterogeneous graphs. Drug-side effect heterogeneous graphs are constructed using drug-side effect associations, drug-disease associations and drug chemical substructures. Based on a graph attention network, Zhao et al. Zhao et al. (2021) developed a prediction model for drug-side effect frequencies that integrated information on similarity, known drug-side effect frequencies, and word embeddings. The above deep learning-based method is a kind of pairwise learning. To keep the sample balanced, this group selected the positive sample from trusted databases and the negative sample by random sampling. Such a treatment, result in a certain loss of information and introduces noise into in label.

Drug-side effect prediction is a classic link prediction problem Yuan et al. (2019). To solve this kind of problem, many multi-view methods have been proposed in recent years Ding et al. (2021); Zou et al. (2019). Among these method, the most commonly used multi-view strategy is the multiple kernel learning (MKL) method Wang et al. (2021); Xu et al. (2021); Guo et al. (2021); Qian et al. (2022a); Wang et al. (2023b), which combines kernels corresponding to different views linearly or non linearly. MKL-KroneckerRLS Ding et al. (2019) combines diversified information using Centered Kernel Alignment-based Multiple Kernel Learning (CKA-MKL). Based on the optimal kernel, Kronecker regularized least squares (Kro-RLS) was used to classify drug-side effect pairs. Kron-RLS with pairwise MKL (Kron-RLS+pairwiseMKL) Cichonska et al. (2018) constructs multiple pairwise kernels, and its weights are also determined by CKA-MKL. In Kron-RLS with self-weighted MKL (Kron-RLS+selfMKL) Nascimento et al. (2016), the weights indicating the importance of individual kernels are calculated automatically to select the more relevant kernels.

It must be noted, however, that the above methods always rely on MKL to learn an optimal kernel from predefined kernels, which may result in some important information being lost. Multiple information fusion during the training process enables the model to explore all views while being allowed to model one view differently. This framework has been applied to classification models Houthuys & Suykens (2021); Houthuys et al. (2018); Qian et al. (2022b); Xie & Sun (2020) and clustering modelsLv et al. (2021); Houthuys et al. (2018); Wang et al. (2023a). In this work, we apply this technique to the Kron-RLS algorithm. Due to its fast and scalable nature. The proposed method is named Multiple Kronecker RLS fusion-based link propagation (MKronRLSF-LP). Our work's main contributions are listed as follows:

(1) We extend Kron-RLS to the multiple information fusion setting by finding the consensus partition and multiple graph Laplacian constraint. Specifically, we generate multiple partitions by normal Kron-RLS and adaptively learn a weight for each partition to control its contribution to the shared partitions. This work was conducted with the aim of fusing partitions while still allowing for some flexibility in modeling the single information. Furthermore, multiple graph Laplacian regularization is adopted to boost the performance of semi-supervised learning. Both settings co-evolve toward better performance.

(2) To fuse the features of multiple information more reasonably, we design an iterative optimization algorithm to effectively fuse multiple Kron-RLS submodels and obtain the final predictive model of drug-side effects. In the whole optimization, we avoid explicit computation of any pairwise matrices, which makes our method suitable for solving problems in large pairwise spaces.

(3) The proposed method can address the general link prediction problem; it is empirically tested on four real drug-side effect datasets, which are more sparse. The results show that MKronRLSF-LP can achieve excellent classification results and outperform other competitive methods.

The rest of this paper is organized as follows. Section 2 provides a description of the drug-side effect prediction problem. Section 3 reviews related work about MKronRLSF-LP. Section 4 comprehensively presents the proposed MKronRLSF-LP. After reporting the experimental results in Section 5, we conclude this paper and mention future work in Section 6.

2 Problem description

Identification of drug-side effects is an example of the link prediction problem, which has the aim of predicting how likely it is that there is a link between two arbitrary nodes in a network. This problem can also be seen as a recommendation system Jiang et al. (2019); Fan et al. (2021) task.

Let the drug nodes and side effect nodes of a network be $\mathbb{D} = \{d_1, d_2, \ldots, d_N\}$ and $\mathbb{S} = \{s_1, s_2, \ldots, s_M\}$, respectively. We denote the number of drug and side effect nodes by N and M, respectively.

We define an adjacency matrix $\boldsymbol{F} \in \mathbb{R}^{N \times M}$ to represent the associations between drugs and side effects. Each element of $\boldsymbol{F}$ is defined as $\boldsymbol{F}_{i,j} = 1$ if the node pair (d_i, s_j) is linked and $\boldsymbol{F}_{i,j} = 0$ otherwise.

The link prediction has the aim of predicting whether a link exists for the unknown state node pair $(d_i, s_j) \in \mathbb{D} \times \mathbb{S}$. Thus, it is a classification problem. Most methods use regression algorithms to predict a score (ranging from 0-1), which we call the link confidence. Then, a class of 0 or 1 is assigned to the predicted score by the threshold. Higher link confidence indicates a greater probability of the link existing, while lower values indicate the opposite. We define a new matrix $\hat{\boldsymbol{F}}$, which is estimated by the prediction model. Each of elements $\hat{\boldsymbol{F}}_{i,j}$ represents the predicted link confidence for the node pair (d_i, s_j). Figure 1 summarizes the link prediction problem discussed in this paper.

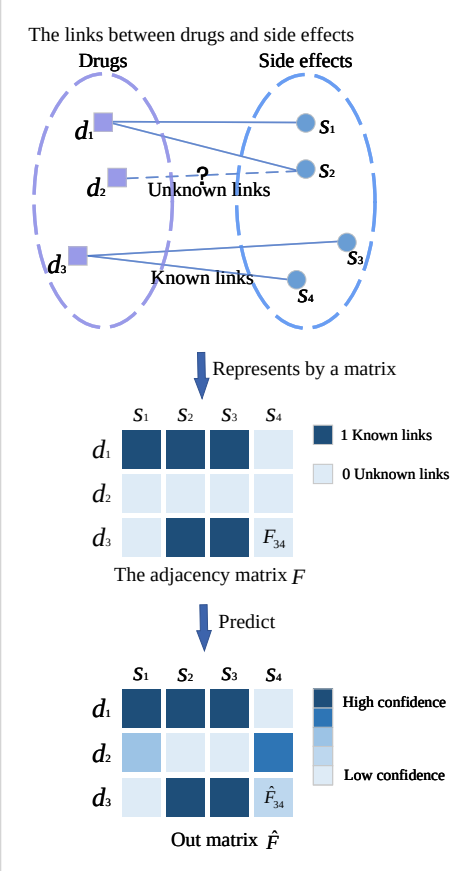

Figure 1: Visualization of drug-side effect association problems.

3 Related work

3.1 Regularized Least Squares

The objective function of Regularized Least Squares (RLS) regression is:

$$\arg\min_{f} \frac{1}{2} \left\| \boldsymbol{F} - f\left(\boldsymbol{K}\right) \right\|_F^2 + \frac{\lambda}{2} \left\| f \right\|_K^2, \tag{1}$$

where λ is a regularization parameter, $\|f\|_K$ denotes the RKHS norm Kailath (1971) of $f(\cdot)$. $f(\cdot)$ is the prediction function and be defined as:

$$f\left(\boldsymbol{K}\right) = \boldsymbol{K}\boldsymbol{a}, \tag{2}$$

where $\boldsymbol{a}$ is the solution of the model, $\boldsymbol{F}$ is a kernel matrix with elements

$$\boldsymbol{K}_{i,j} = k\left(d_i, d_j\right)\left(i, j = 1, \ldots, N\right), \tag{3}$$

and k represents the kernel function.

By formulating the stationary points of Equation 1 and elimination the unknown parameters $\boldsymbol{a}$, the following solution is obtained

$$\hat{\boldsymbol{F}} = \boldsymbol{K}(\boldsymbol{K} + \lambda \boldsymbol{I}_N)^{-1}\boldsymbol{F}. \tag{4}$$

There is only one kind of feature space considered in this model. In the drug-side effect identification problem, there are two feature spaces: the drug space and the side effect space.

3.2 Kronecker Regularized Least Squares

Combining the kernels of the two spaces into a single large kernel that directly relates drug-side effect pairs would be a better option. Kronecker product kernel Hue & Vert (2010) is used for this. Given the drug kernel $\boldsymbol{K}_D$ and side effect kernel $\boldsymbol{K}_S$, then we have the kronecker product kernel

$$\boldsymbol{K} = \boldsymbol{K}_S \otimes \boldsymbol{K}_D, \tag{5}$$

where the $\otimes$ indicates the Kronecker product Laub (2004). By applying the Kronecker product kernel to RLS, the objective function of Kronecker Regularized Least Squares (Kron-RLS) is botained:

$$\arg\min_f \ \frac{1}{2}\left\|\mathrm{vec}\left(\boldsymbol{F}\right) - f\left(\boldsymbol{K}\right)\right\|_F^2 + \frac{\lambda}{2}\left\|f\right\|_K^2, \tag{6}$$

where $\mathrm{vec}\left(\cdot\right)$ is the vectorization operating function. By setting the derivative of Equation 6 *w.r.t* $\boldsymbol{a}$ to zero, we obtain:

$$\boldsymbol{a} = \left(\boldsymbol{K} + \lambda \boldsymbol{I}_{NM}\right)^{-1}\mathrm{vec}\left(\boldsymbol{F}\right). \tag{7}$$

Obviously, it needs calculating the inverse of $(\boldsymbol{K} + \lambda \boldsymbol{I}_{NM})$ with size of $NM \times NM$, whose time complexity is $O\left(N^3M^3\right)$. Thus, a well-known theorem Raymond & Kashima (2010); Laub (2004) is proposed to obtain the approximate inverse.

It is well known that the kernel Liu et al. (2023); Pekalska & Haasdonk (2008) matrices are positive semi-definite matrices, they can be eigen decomposed, $\boldsymbol{K}_D = \boldsymbol{V}_D\boldsymbol{\Lambda}_D\boldsymbol{V}_D^T$ and $\boldsymbol{K}_S = \boldsymbol{V}_S\boldsymbol{\Lambda}_S\boldsymbol{V}_S^T$. According to the theorem Raymond & Kashima (2010); Laub (2004), the eigenvectors of the Kronecker product kernel $\boldsymbol{K}$ is the $\boldsymbol{V} = \boldsymbol{V}_S \otimes \boldsymbol{V}_D$. Define the matrix $\boldsymbol{\Lambda}$ to be either $\boldsymbol{\Lambda}_{i,j} = [\boldsymbol{\Lambda}_S]_{i,i} \times [\boldsymbol{\Lambda}_D]_{j,j}$. The eigenvalues of $\boldsymbol{K}$ is $\mathrm{diag}\left(\mathrm{vec}\left(\boldsymbol{\Lambda}\right)\right)$. The matrix $\boldsymbol{K} + \lambda \boldsymbol{I}_{NM}$ has the same eigenvactors $\boldsymbol{V}$, and eigenvalues $\mathrm{diag}\left(\mathrm{vec}\left(\boldsymbol{\Lambda} + \lambda \boldsymbol{1}\right)\right)$. Then, we can rewrite Equation 7 as:

$$\boldsymbol{K}(\boldsymbol{K} + \lambda \boldsymbol{I}_{NM})^{-1}\mathrm{vec}\left(\boldsymbol{F}\right) = \boldsymbol{V}\mathrm{diag}(\mathrm{vec}\left(\boldsymbol{\Lambda}\right))\boldsymbol{V}^T\boldsymbol{V}\mathrm{diag}(\mathrm{vec}\left(\boldsymbol{\Lambda} + \lambda \boldsymbol{1}\right))^{-1}\boldsymbol{V}^T\mathrm{vec}\left(\boldsymbol{F}\right). \tag{8}$$

Since $\boldsymbol{V}^T\boldsymbol{V} = \boldsymbol{I}_{NM}$ and $\mathrm{diag}(\mathrm{vec}\left(\boldsymbol{\Lambda}\right))\mathrm{diag}(\mathrm{vec}\left(\boldsymbol{\Lambda} + \lambda \boldsymbol{1}\right))^{-1}$ is also a diagonal matrix, we further simplify Equation 8 and get

$$\boldsymbol{K}(\boldsymbol{K} + \lambda \boldsymbol{I}_{NM})^{-1}\mathrm{vec}\left(\boldsymbol{F}\right) = \boldsymbol{V}\mathrm{diag}(\mathrm{vec}\left(\boldsymbol{J}\right))\boldsymbol{V}^T\mathrm{vec}\left(\boldsymbol{F}\right), \tag{9}$$

where the matrix $\boldsymbol{J}$ to be either

$$\boldsymbol{J}_{i,j} = \frac{\boldsymbol{\Lambda}_{i,j}}{\boldsymbol{\Lambda}_{i,j} + \lambda}. \tag{10}$$

Using the vec-tricks techniques $((\boldsymbol{A} \otimes \boldsymbol{B})\,\mathrm{vec}\left(\boldsymbol{C}\right) = \mathrm{vec}\left(\boldsymbol{B}\boldsymbol{C}\boldsymbol{A}^T\right))$, we further simplify Equation 8. Then, we get

$$\hat{\boldsymbol{F}} = \boldsymbol{V}_D\left(\boldsymbol{J} \odot \left(\boldsymbol{V}_D^T\boldsymbol{F}\boldsymbol{V}_S\right)\right)^T\boldsymbol{V}_S^T, \tag{11}$$

where $\odot$ represents the Hadamard product. The computational time of this optimization method is $O\left(N^3 + M^3\right)$, which is much less than $O\left(N^3M^3\right)$.

3.3 Kronecker Regularized Least Squares with Multiple Kernel Learning

Kron-RLS is a kind of kernel method. It can be difficult for nonexpert users to choose an appropriate kernel. To address such limitations, Multiple Kernel Learning (MKL) Gönen & Alpaydın (2011) is proposed. Since kernels in MKL can naturally correspond to different views, MKL has been applied with great success to cope with the multi-view data Wang et al. (2021); Xu et al. (2021); Guo et al. (2021); Qian et al. (2022a); Wang et al. (2023b) by combining kernels appropriately.

Given predefined base kernels $\left\{\boldsymbol{K}_D^i\right\}_{i=1}^P$ and $\left\{\boldsymbol{K}_S^j\right\}_{j=1}^Q$ from drug feature space and side effect feature space, respectively. These kernels can be built from different types or views. The optimal kernel can be combined by a linear function corresponding to the base kernels:

$$\boldsymbol{K}_D^{opt} = \sum_{i=1}^{P} w^i \boldsymbol{K}_D^i. \tag{12}$$

Usually, an additional constraint is imposed on the corresponding combination coefficient w to control its structure:

$$\sum_{i=1}^{P} w^i = 1, w^i \geq 0, i = 1, \ldots, P. \tag{13}$$

The optimal side effect kernel $\boldsymbol{K}_S^{opt}$ is omitted.

Based on MKL method, Ding et al. Ding et al. (2019) and Nascimento et al. Nascimento et al. (2016) developed Kron-RLS based MKL methods, called Kron-RLS with CKA-MKL and Kron-RLS with selfMKL, respectively. Kron-RLS with CKA-MKL combines diversified information using Centered Kernel Alignment-based Multiple Kernel Learning (CKA-MKL). In Kron-RLS with selfMKL, the weights indicating the importance of individual kernels are calculated automatically to select the more relevant kernels. The final decision function of both methods is given by:

$$\operatorname{vec}\left(\hat{\boldsymbol{F}}\right) = \left(\boldsymbol{K}_S^{opt} \otimes \boldsymbol{K}_D^{opt}\right)\left(\boldsymbol{K}_S^{opt} \otimes \boldsymbol{K}_D^{opt} + \lambda \boldsymbol{I}_{NM}\right)^{-1} \operatorname{vec}\left(\boldsymbol{F}\right). \tag{14}$$

4 Proposed method

Existing multi view fusion methods based on Kron-RLS all follow MKL framework. These methods optimize the optimal pairwise kernel as a linear combination of a set of base kernels. Prior to training, all views are fused, and information is not shared during training phase. This is typical early fusion technology. Our proposal addresses this limitation by fusing multi-view information in a consensus partition. Compared with MKL framework, the advantage of the proposed method is that it allows sub partitions to have a certain degree of freedom to model the single information. Further, multiple graph Laplacian regularization is introduced into the consensus partition to boost performance. Fig. 2 illustrates the main procedure of MKronRLSF-LP.

4.1 The construction of kernel matrix

Kron-RLS is a kind of kernel method. We construct drug kernels using five different kinds of functions.

Gaussian Interaction Profile (GIP):

$$\left[\boldsymbol{K}_{GIP,D}\right]_{i,j} = \exp\left(-\gamma \|d_i - d_j\|^2\right), \tag{15}$$

where γ is the gaussian kernel bandwidth and $\gamma = 1$.

Cosine Similarity (COS):

$$\left[\boldsymbol{K}_{COS,D}\right]_{i,j} = \frac{d_i^T d_j}{|d_i|\,|d_j|}. \tag{16}$$

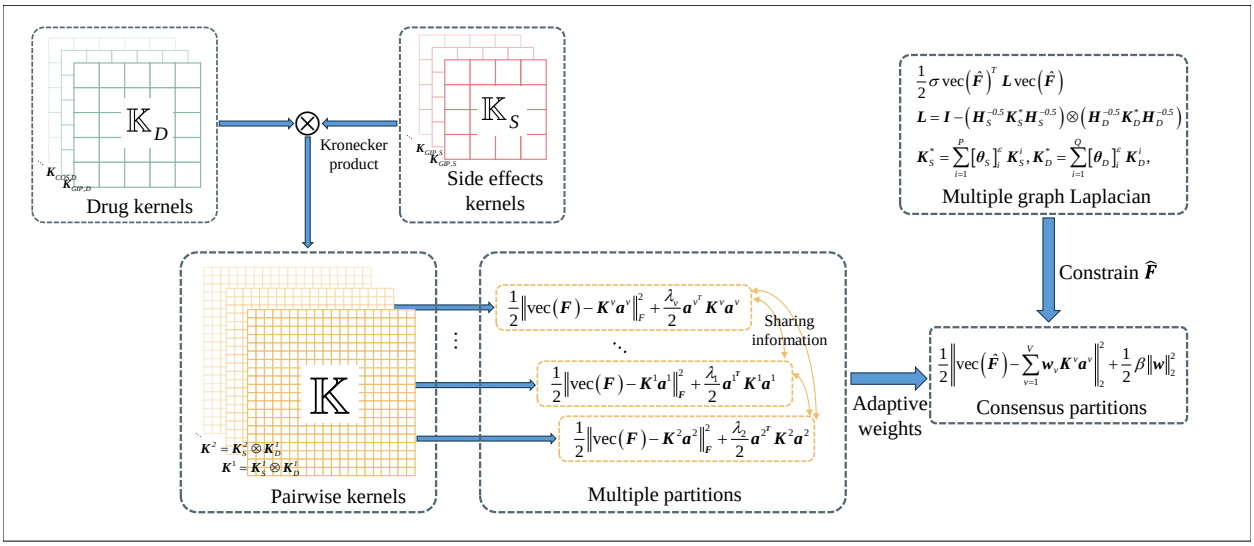

Figure 2: Framework diagram of MKronRLSF-LP. MKronRLSF-LP allow the multiple partitions have a degree of freedom to model the single information and introduce a multiple graph Laplacian regularization into consensus partition.

Correlation coefficient (Corr):

$$[\boldsymbol{K}_{Corr,D}]_{i,j} = \frac{\mathrm{Cov}\left(d_i, d_j\right)}{\sqrt{\mathrm{Var}\left(d_i\right)\mathrm{Var}\left(d_j\right)}}. \tag{17}$$

Normalized Mutual Information (NMI):

$$[\boldsymbol{K}_{NMI,D}]_{i,j} = \frac{\mathrm{Q}\left(d_i, d_j\right)}{\sqrt{\mathrm{H}\left(d_i\right)\mathrm{H}\left(d_j\right)}}, \tag{18}$$

where $\mathrm{Q}\left(d_i, d_j\right)$ is the mutual information of d_i and d_j. $\mathrm{H}\left(d_i\right)$ and $\mathrm{H}\left(d_j\right)$ are the entropies of d_i and d_j, respectively.

Neural Tangent Kernel (NTK):

$$[K_{NTK,D}]_{i,j} = \mathbb{E}_{\theta\sim w}\left[f_{NTK}\left(\theta, d_i\right), f_{NTK}\left(\theta, d_j\right)\right], \tag{19}$$

where f_{NTK} is a fully connected neural network and θ is collection of parameters in this network.

Similarity, we construct the side effect kernels ($\boldsymbol{K}_{GIP,S}$, $\boldsymbol{K}_{COS,S}$, $\boldsymbol{K}_{Corr,S}$, $\boldsymbol{K}_{NMI,S}$, $\boldsymbol{K}_{NTK,S}$) in side effect space.

4.2 The MKronRLSF-LP model

Let us define two sets of base kernel sets separately:

$$\mathbb{K}_D = \left\{\boldsymbol{K}_D^1, \ldots, \boldsymbol{K}_D^P\right\}, \tag{20a}$$

$$\mathbb{K}_S = \left\{\boldsymbol{K}_S^1, \ldots, \boldsymbol{K}_S^Q\right\}, \tag{20b}$$

where P and Q represents the numbers of drug and side effect kernels, respectively. Based on the $\boldsymbol{K}_D$ and $\boldsymbol{K}_S$, we can get a set of pairwise kernels:

$$\mathbb{K} = \left\{\boldsymbol{K}^1 = \boldsymbol{K}_S^1 \otimes \boldsymbol{K}_D^1, \ldots, \boldsymbol{K}^V = \boldsymbol{K}_S^P \otimes \boldsymbol{K}_D^Q\right\}, \tag{21}$$

where V denotes the numbers of base pairwise kernels. Obviously, V is equal to $P \times Q$.

By using multiple partitions, we can manipulate multiple views in a partition space, which enhances the robustness of the model. The following ensemble KronRLS model is obtained

$$\arg\min_{\boldsymbol{a}^v} \sum_{v=1}^{V} \left(\frac{1}{2} \left\| \mathrm{vec}\left(\boldsymbol{F}\right) - \boldsymbol{K}^v \boldsymbol{a}^v \right\|_2^2 + \frac{\lambda_v}{2} \boldsymbol{a}^{v^T} \boldsymbol{K}^v \boldsymbol{a}^v \right). \tag{22}$$

We define the consensus result as $\hat{\boldsymbol{F}}$. It is a weighted linear combination of results from multiple distinct views. A variable $\boldsymbol{w}_v$ is introduced for view v which characterizes its importance, which is calculated based on the training error. To prevent sparse situations, we employ $\|\cdot\|_2^2$ to smooth the weights. Then, we have the following optimization problem

$$\begin{aligned} \arg\min_{\hat{\boldsymbol{F}}, \boldsymbol{a}^v, \boldsymbol{w}} \; & \frac{1}{2} \left\| \mathrm{vec}\left(\hat{\boldsymbol{F}}\right) - \sum_{v=1}^{V} \boldsymbol{w}_v \boldsymbol{K}^v \boldsymbol{a}^v \right\|_2^2 + \mu \sum_{v=1}^{V} \left(\frac{\boldsymbol{w}_v}{2} \left\| \mathrm{vec}\left(\boldsymbol{F}\right) - \boldsymbol{K}^v \boldsymbol{a}^v \right\|_F^2 + \frac{\lambda_v}{2} \boldsymbol{a}^{v^T} \boldsymbol{K}^v \boldsymbol{a}^v \right) + \frac{1}{2} \beta \left\| \boldsymbol{w} \right\|_2^2 \\ & s.t. \sum_{v=1}^{V} \boldsymbol{w}_v = 1, \boldsymbol{w}_v \geq 0, v = 1, \ldots, V. \end{aligned} \tag{23}$$

A natural assumption could be if $\boldsymbol{K}^v$ can capture the correlation, then the node pair sharing the same labels should be kept close together. This means any two pair nodes with same labels have a higher similarity. That is, the pair node labels with stronger correlations are assumed to be closer to each other in the original space. This is analogous to the Laplacian operator on manifolds Belkin et al. (2006); Chao & Sun (2019); Jiang et al. (2023). Here, we apply multiple graph Laplacian regularization to Equation 23, which can effectively explore multiple different views and boost the performance of $\hat{\boldsymbol{F}}$. Specifically, the Kronecker product Laplacian matrix is calculated from the optimal drug and side effect similarity matrix, which are weighted linear combinations of multiple related kernel matrices. The weight of each kernel can be adaptively optimized during the training process. The optimization problems for MKronRLSF-LP can be formulated as:

$$\begin{aligned} \arg\min_{\hat{\boldsymbol{F}}, \boldsymbol{a}^v, \boldsymbol{w}, \boldsymbol{\theta}_D, \boldsymbol{\theta}_S} \; & \frac{1}{2} \left\| \mathrm{vec}\left(\hat{\boldsymbol{F}}\right) - \sum_{v=1}^{V} \boldsymbol{w}_v \boldsymbol{K}^v \boldsymbol{a}^v \right\|_2^2 + \mu \sum_{v=1}^{V} \left(\frac{\boldsymbol{w}_v}{2} \left\| \mathrm{vec}\left(\boldsymbol{F}\right) - \boldsymbol{K}^v \boldsymbol{a}^v \right\|_2^2 + \frac{\lambda^v}{2} \boldsymbol{a}^{v^T} \boldsymbol{K}^v \boldsymbol{a}^v \right) + \frac{1}{2} \beta \left\| \boldsymbol{w} \right\|_2^2 \\ & + \frac{1}{2} \sigma \mathrm{vec}\left(\hat{\boldsymbol{F}}\right)^T \boldsymbol{L} \mathrm{vec}\left(\hat{\boldsymbol{F}}\right) \\ & s.t. \sum_{v=1}^{V} \boldsymbol{w}_v = 1, \boldsymbol{w}_v \geq 0, v = 1, \ldots, V, \\ & \boldsymbol{L} = \boldsymbol{I}_{NM} - \left(\boldsymbol{H}_S^{-0.5} \boldsymbol{K}_S^* \boldsymbol{H}_S^{-0.5} \right) \otimes \left(\boldsymbol{H}_D^{-0.5} \boldsymbol{K}_D^* \boldsymbol{H}_D^{-0.5} \right), \\ & \boldsymbol{K}_S^* = \sum_{i=1}^{Q} [\boldsymbol{\theta}_S]_i^{\varepsilon} \boldsymbol{K}_S^i, \boldsymbol{K}_D^* = \sum_{i=1}^{P} [\boldsymbol{\theta}_D]_i^{\varepsilon} \boldsymbol{K}_D^i, \\ & \sum_{i=1}^{Q} [\boldsymbol{\theta}_S]_i = 1, [\boldsymbol{\theta}_S]_i \geq 0, i = 1, \ldots, Q, \sum_{i=1}^{P} [\boldsymbol{\theta}_D]_i = 1, [\boldsymbol{\theta}_D]_i \geq 0, i = 1, \ldots, P. \end{aligned} \tag{24}$$

where $\boldsymbol{L}$ is a normalized laplacian matrix, $\boldsymbol{H}_S$ and $\boldsymbol{H}_D$ are diagonal matrix with the jth diagonal elements as $\sum_k [\boldsymbol{K}_S^*]_{j,k}$ and $\sum_k [\boldsymbol{K}_D^*]_{j,k}$, respectively. And, $\varepsilon > 1$, guaranteeing each graph has a particular contribution to the Laplacian matrix.

Due to the lack of space, we present optimization algorithm of the Equation 24 in Appendix Section A.1.

5 Experiments

In this section, the performance of MKronRLSF-LP is shown, and we make comparisons with baseline methods and other drug-side effect predictors.

5.1 Dataset

Table 1: Summary of the real drug-side effect datasets.

Name	Drug	Side effect	Zero of rates	Reference
Liu	832	1385	94.86%	Cheng et al. (2013)
Pau	888	1385	95.03%	Pauwels et al. (2011)
Miz	658	1339	94.43%	Sayaka et al. (2012)
Luo	708	4192	97.30%	Luo et al. (2017)

Four real drug-side effect datasets are used to assess the effectiveness of our proposed method. Table 1 summarizes information about the datasets. We can see that these four datasets are sparse. In other words, there are fewer positive samples than negative samples. Thus, drug-side effect prediction can be viewed as a classification problem with extremely imbalanced data.

5.2 Parameter setting

In this paper, the objective function 24 contains the following regularization parameters: μ, β, σ, ε and $\lambda^v, v = 1, \ldots, V$. To find the right combinations of the regularization parameters of MKronRLSF-LP to give the best performance, the grid search method is performed on the Pau dataset. The optimal parameters with the best AUPR are selected.

We first select $\lambda^v, v = 1, \ldots, V$ by the relative pairwise kernel with a single view Kron-RLS model. For each parameter λ^v, we select it in the range from 2^{-5} to 2^5 with step 2^1. The optimal parameters λ^v are shown in Table 7. According to a previous studyShi et al. (2019), the performance is not affected by parameter ε, so it is set to 2. Then, we fix $\lambda^v, v = 1, \ldots, V$ at the best values and tune μ, β, σ from within the range 2^{-10} to 2^0 with step 2^1. The optimal regularization parameters are $\mu = 2^{-7}$, $\beta = 2^0$ and $\sigma = 2^{-8}$.

5.3 Baseline methods

In this work, we compare MKronRLSF-LP with the following baseline methods: BSV, Comm Kron-RLSPerrone & Cooper (1995), Kron-RLS+CKA-MKLDing et al. (2019), Kron-RLS+pairwiseMKLCichonska et al. (2018), Kron-RLS+self-MKLNascimento et al. (2016), MvGRLPDing et al. (2021) and MVGCNFu et al. (2022). Due to the lack of space, we present details of these baseline methods in Appendix Section A.3. For a fair comparison, the same input as our method is fed into these baseline methods. To achieve the best performance, we also adopt 5-fold CV on the Pau dataset to tune the parameters.

5.4 Threshold finding

Because the MKronRLSF-LP and baseline methods only output the value of regression, we apply a threshold finding operation. A trend of F_{score}, *Recall* and *Precision* with different thresholds over four datasets is shown in Fig. 3. While the threshold of prediction rises, the values of *Recall* is rising. Oppositely, $Psecision$ is falling. The F_{score} is the harmonic mean of the *Recall* and *Precision*. It thus symmetrically represents both *Recall* and *Precision* in one metric. Here, we find the optimal threshold under maximizing the value of F_{score}. Table 8 summarizes the thresholds of different baseline methods on different datasets.

5.5 Comparison with baseline methods

We conduct a five fold cross-validation procedure (5-fold CV) to evaluate the performance of our method versus the baseline method. To further provide a fair and comprehensive comparison, each algorithm is iterated 10 times with different cross index, and then the mean values and standard deviations are reported in Table 2. The best single view is $K_{GIP,D} \otimes K_{NTK,S}$, which is selected by 5-fold CV on the Pau dataset.

First, we observe that the proposed method has the best AUPR and F_{score} on all datasets. Especially, the proposed method has a higher AUPR and F_{score} than BSV on datasets. This indicates the improvement in

Table 2: Prediction performance comparison of baseline methods on four datasets.

Dataset	Methods	AUPR(%)	AUC(%)	*Recall*(%)	*Precision*(%)	F_{score}(%)
Liu	BSV	60.12±1.12	93.22±1.63	58.77±0.33	59.09±0.49	58.52±0.23
	Comm Kron-RLS	65.63±1.95	94.11±1.45	61.63±0.33	61.9±1.37	61.57±1.65
	Kron-RLS +CKA-MKL	65.92±0.43	92.51±0.08	62.11±0.43	63.09±0.56	62.59±0.41
	Kron-RLS +pairwiseMKL	62.03±0.44	**95.01±0.06**	**65.39±0.24**	54.46±0.30	59.43±0.21
	Kron-RLS +self-MKL	65.02±0.47	92.1±0.10	60.97±0.57	**63.12±0.61**	62.03±0.52
	MvGRLP	66.32±0.45	94.29±0.08	63.56±0.46	60.87±0.62	62.18±0.39
	MvGCN	62.69±1.81	94.01±0.87	60.81±0.37	60.33±1.31	60.48±1.15
	MKronRLSF-LP	**68.02±0.44**	94.78±0.13	65.18±0.93	61.27±1.08	**63.02±0.43**
Pau	BSV	65.26±0.98	94.57±0.34	62.54±0.5	60.77±1.27	60.65±0.73
	Comm Kron-RLS	65.63±0.36	94.78±0.13	64.01±0.38	60.05±0.49	61.01±0.27
	Kron-RLS +CKA-MKL	65.49±0.37	92.39±0.13	61.65±0.40	**63.22±0.51**	62.42±0.27
	Kron-RLS +pairwiseMKL	63.48±0.39	**95.02±0.07**	**78.1±0.26**	45.01±0.48	57.11±0.36
	Kron-RLS +self-MKL	64.11±1.75	91.94±0.25	62.37±0.29	60.97±1.57	61.65±0.79
	MvGRLP	66.17±0.32	94.42±0.07	62.18±0.38	61.95±0.45	62.06±0.22
	MvGCN	63.51±1.43	94.08±0.49	63.21±0.69	57.94±1.34	60.4±1.78
	MKronRLSF-LP	**67.81±0.37**	94.81±0.18	65.72±3.58	60.65±3.75	**62.87±0.48**
Miz	BSV	56.58±2.33	90.71±2.06	62.76±0.69	53.94±2.31	55.39±2.33
	Comm Kron-RLS	58.08±1.07	91.36±1.25	62.37±0.81	55.16±1.99	56.54±1.77
	Kron-RLS +CKA-MKL	66.92±0.44	92.58±0.14	62.62±0.52	**64.3±0.46**	61.45±0.44
	Kron-RLS +pairwiseMKL	62.13±0.29	**94.70±0.11**	63.78±0.47	56.26±0.42	59.79±0.30
	Kron-RLS +self-MKL	65.84±0.43	92.06±0.16	63.63±0.48	61.77±0.52	60.68±0.43
	MvGRLP	66.68±0.35	94.10±0.12	63.46±0.43	61.82±0.30	62.63±0.29
	MvGCN	62.17±1.90	93.35±1.73	59.54±0.43	60.74±1.78	59.76±1.95
	MKronRLSF-LP	**68.35±0.38**	94.47±0.09	**65.15±2.77**	62.10±3.19	**63.45±0.53**
Luo	BSV	60.40±0.40	94.40±0.11	58.28±0.41	58.68±0.46	58.48±0.39
	Comm Kron-RLS	54.19±1.36	91.92±4.01	57.64±2.46	53.16±1.97	52.99±1.54
	Kron-RLS +CKA-MKL	60.87±0.36	92.03±0.15	55.55±0.34	**64.15±0.46**	59.54±0.36
	Kron-RLS +pairwiseMKL	50.29±0.29	94.37±0.10	55.66±0.39	45.97±0.39	50.35±0.31
	Kron-RLS +self-MKL	22.29±1.57	79.74±1.62	56.62±1.47	20.91±1.64	28.23±1.15
	MvGRLP	61.76±0.45	94.08±0.07	58.70±0.40	60.05±0.61	58.37±0.42
	MvGCN	61.18±0.41	**94.54±0.1**	57.94±0.37	61.26±0.48	51.07±0.38
	MKronRLSF-LP	**63.32±0.58**	94.07±0.14	**59.43±0.95**	61.58±1.22	**60.47±0.39**

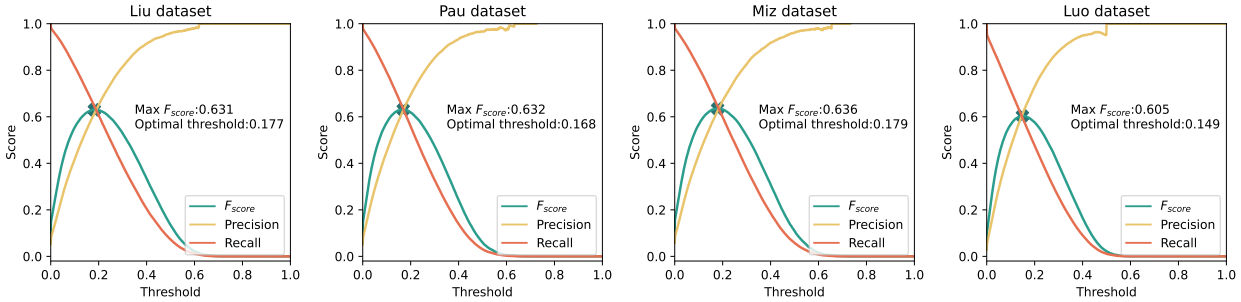

Figure 3: Results (MKronRLSF-LP) for F_{score}, *Recall* and *Precision* of different thresholds.

Table 3: Prediction performance comparison of other drug-side effect predictors on Liu datasets.

Methods	AUPR(%)	AUC(%)	*Recall*(%)	*Precision*(%)	F_{score}(%)
Liu's method	28.0	90.7	**67.5**	34.0	45.2
Cheng's method	59.2	92.2	59.0	55.7	56.9
RBMBM	61.6	94.1	61.5	57.4	59.4
INBM	64.1	93.4	60.7	<u>60.4</u>	60.6
Ensemble model	66.1	<u>94.8</u>	62.3	61.1	<u>61.7</u>
MKL-LGC[a]	<u>67.0</u>	**95.1**	-	-	-
NDDSA with sschem[c]	60.5	94.1	57.9	56.4	57.1
NDDSA without sschem[c]	60.4	94.0	57.4	56.8	57.1
MKronRLSF-LP	**68.2**	94.7	<u>63.8</u>	**62.5**	**63.1**

- represents not available; the bold and underlined values represent the best and second performance measure in each column, respectively;
a and b represents the results are derived from Ding et al. (2018) and Shabani-Mashcool et al. (2020), respectively.

using multiple views. The simple coupling frameworks BSV and Comm perform well on the Pau dataset. However, BSV and Comm cannot perform as well on other datasets, which indicates that the simple fusion schemes are sensitive to the dataset and not robust. Furthermore, Kron-RLS+pairwiseMKL achieves the highest AUC of 95.01%, 95.02% and 94.70% on the Liu, Pau and Miz datasets, respectively. This shows slight improvements of 0.23%, 0.21% and 0.23% over our method, respectively. As we discussed in Section 5.1, drug-side effect prediction is an extremely imbalanced classification problem. The AUC can be considered as the probability that the classifier will rank a randomly chosen positive instance higher than a randomly chosen negative instance. Therefore, the AUC is not an important metric for predicting drug side effects.

Another interesting, observation is that MKronRLSF-LP outperforms other MKL strategy methods in comparison. For example, it exceeds the best MKL method (CKA-MKL) by 2.1%, 2.32%, 1.43%, 2.51% in terms of AUPR on Liu, Pau, Miz and Luo dataset, respectively. These results verify the effectiveness of the consensus partition and multiple graph Laplacian constraint.

In summary, the above experimental results demonstrate the effectiveness of MKronRLSF-LP to other baseline methods. We attribute the superiority of MKronRLSF-LP as three aspects: (1) The consensus partition is derived through joint fusion of weighted multiple partitions; (2) MKronRLSF-LP utilizes the multiple graph Laplacian regularization to constrain the consensus predicted value $\hat{\boldsymbol{F}}$, which makes the consensus partition is robust; (3) Unlike existing MKL methods, the proposed MKronRLSF-LP fuses multiple pairwise kernels at the partition level. It is these three factors that contribute to the improvement in prediction performance.

Table 4: Prediction performance comparison of other drug-side effect predictors on Pau datasets.

Methods	AUPR(%)	AUC(%)	*Recall*(%)	*Precision*(%)	F_{score}(%)
Pau's method[a]	38.9	89.7	51.7	36.1	42.5
Liu's method	34.7	92.1	**64.6**	40.0	49.5
Cheng's method	58.8	82.3	58.3	55.0	56.6
RBMBM	61.3	94.1	60.8	57.7	59.2
INBM	64.1	93.4	60.8	60.5	60.7
Ensembel model	66.0	<u>94.9</u>	62.4	<u>61.2</u>	<u>61.6</u>
MKL-LGC[b]	<u>66.8</u>	**95.2**	-	-	-
NDDSA with sschem[c]	60.3	94.2	59.3	54.9	57.0
NDDSA without sschem[c]	60.3	94.1	58.2	55.9	57.0
MKronRLSF-LP	**67.9**	94.7	<u>63.4</u>	**62.9**	**63.2**

- represents not available; the bold and underlined values represent the best and second performance measure in each column, respectively;
a, b and c represents the results are derived from Zhang et al. (2016), Ding et al. (2018) and Shabani-Mashcool et al. (2020), respectively.

Table 5: Prediction performance comparison of other drug-side effect predictors on Miz datasets.

Methods	AUPR(%)	AUC(%)	*Recall*(%)	*Precision*(%)	F_{score}(%)
Miz's method[a]	41.2	89.0	52.7	38.7	44.6
Liu' method	36.3	91.8	**64.0**	41.5	50.5
Cheng's method	56.0	92.3	58.4	56.8	57.6
RBMBM	61.7	93.9	60.5	58.8	59.6
INBM	64.6	93.2	61.6	60.5	61.1
Ensemble model	66.6	<u>94.6</u>	62.4	<u>61.9</u>	<u>62.2</u>
MKL-LGC[b]	<u>67.3</u>	**94.8**	-	-	-
NDDSA with sschem[c]	60.6	93.9	58.8	56.3	57.5
NDDSA without sschem[c]	60.7	93.6	60.0	55.5	57.6
MKronRLSF-LP	**68.5**	94.5	<u>63.0</u>	**64.2**	**63.6**

- represents not available; the bold and underlined values represent the best and second performance measure in each column, respectively;
a, b and c represents the results are derived from Zhang et al. (2016), Ding et al. (2018) and Shabani-Mashcool et al. (2020), respectively.

Table 6: Prediction performance comparison of other drug-side effect predictors on Luo datasets.

Methods	AUPR(%)	AUC(%)	*Recall*(%)	*Precision*(%)	F_{score}(%)
Liu's method	39.4	93.5	**59.6**	48.3	53.3
Cheng's method	53.2	90.9	53.1	52.3	52.7
RBMBM	55.1	93.5	56.1	54.3	55.1
INBM	57.3	91.7	55.8	56.7	<u>56.2</u>
Ensemble model	58.6	93.9	46.1	**68.4**	55.1
MKL-LGC	<u>61.7</u>	<u>94.6</u>	-	-	-
NDDSA with sschem[a]	53.1	94.2	47.6	57.3	52.0
NDDSA without sschem[a]	44.5	93.7	44.7	47.8	46.2
GCRS[b]	27.2	**95.7**	-	-	-
SDPred	22.6	94.6	-	-	-
MKronRLSF-LP	**63.5**	94.1	<u>59.2</u>	<u>61.9</u>	**60.5**

- represents not available; the bold and underlined values represent the best and second performance measure in each column, respectively;
a,b represents the results are derived from Shabani-Mashcool et al. (2020) and Xuan et al. (2022), respectively.

5.6 Comparison with other drug-side effect predictors

A comparison of the proposed drug-side effect prediction method with state-of-the-art methods is also provided. Tables 3,4, 5 and 6 present the results of 5-fold CV in terms of AUPR, AUC, *Recall*, *Precision* and F_{score} on the four datasets, respectively. We have highlighted the best results in bold and underlined the second-best results.

Obviously, MKronRLSF-LP achieves the best prediction results for all datasets (the highest AUPR and F_{score} score on all datasets). GCRS Xuan et al. (2022) and SDPred Zhao et al. (2022) are deep learning-based methods. GCRS constructed multiple heterogeneous graphs and multi-layer convolutional neural networks with attribute-level attention to predict drug-side effect pair nodes. SDPred fuses multiple side informations (including drug chemical structures, drug target, drug word, side effect semantic similarity, side effect word) by feature concatenation and adopt CNN and MLP for the prediction tasks. However, on Luo dataset, GCRS and SDPred perform poorly; this is probably because they are pairwise learning methods and randomly negative sampling to construct the training set. The randomly negative sampling method cannot be guaranteed due to the reliability and quality of negative sample pairs, which results in a certain loss of informationZhang et al. (2015); Ali & Aittokallio (2019). The ensemble model Zhang et al. (2016) combine Liu's method Liu et al. (2012), Cheng's method Cheng et al. (2013), INBM and RBM by the average scoring rule. It is obvious that the results of the ensemble model are significantly improved than the results of the sub-model on four datasets.

6 Conclusion and future work

This paper presents MKronRLSF-LP for drug-side effect prediction. The MKronRLSF-LP method solves the general problem of multi-view fusion-based link prediction by utilizing the consensus partition and multiple graph Laplacian constraint. MKronRLSF-LP allows for some degree of freedom to model the views differently and combination weights for each view to find the consensus partition. Each view's weight is dynamically learned and plays a crucial role in exploring consensus information. It is found that the use of Laplacian regularization enhances semi-supervised learning performance, so a term of multiple graph Laplacian regularization is added to the objective function. Finally, we present an efficient alternating optimization algorithm. The results of our experiments indicate that our proposed methods are superior in terms of their classification results to other baseline algorithms and current drug-side effect predictors.

MKronRLSF-LP uses L_2 loss to measure the quality of approximation. However, the L_2 loss function measure is sensitive to outliers and the interaction matrix contains false zeros. Thus, feature work contain replaces the quadratic form of residues by robust loss, such as LINEX lossTang et al. (2021) and p-power lossChen et al. (2017).

References

Mehreen Ali and Tero Aittokallio. Machine learning and feature selection for drug response prediction in precision oncology applications. *Biophysical reviews*, 11(1):31–39, 2019.

Mikhail Belkin, Partha Niyogi, and Vikas Sindhwani. Manifold regularization: A geometric framework for learning from labeled and unlabeled examples. *Journal of machine learning research*, 7(11), 2006.

Richard H Byrd, Mary E Hribar, and Jorge Nocedal. An interior point algorithm for large-scale nonlinear programming. *SIAM Journal on Optimization*, 9(4):877–900, 1999.

Guoqing Chao and Shiliang Sun. Semi-supervised multi-view maximum entropy discrimination with expectation laplacian regularization. *Information Fusion*, 45:296–306, 2019.

Badong Chen, Lei Xing, Xin Wang, Jing Qin, and Nanning Zheng. Robust learning with kernel mean p-power error loss. *IEEE transactions on cybernetics*, 48(7):2101–2113, 2017.

F. Cheng, W. Li, X. Wang, Y. Zhou, Z. Wu, J. Shen, and Y. Tang. Adverse drug events: database construction and in silico prediction. *Journal of Chemical Information & Modeling*, 53(4):744–752, 2013.

Anna Cichonska, Tapio Pahikkala, Sandor Szedmak, Heli Julkunen, Antti Airola, Markus Heinonen, Tero Aittokallio, and Juho Rousu. Learning with multiple pairwise kernels for drug bioactivity prediction. *Bioinformatics*, 34(13):i509–i518, 2018.

Brianna A Da Silva and Mahesh Krishnamurthy. The alarming reality of medication error: a patient case and review of pennsylvania and national data. *Journal of community hospital internal medicine perspectives*, 6(4):31758, 2016.

Yijie Ding, Jijun Tang, and Fei Guo. Identification of drug-side effect association via semisupervised model and multiple kernel learning. *IEEE journal of biomedical and health informatics*, 23(6):2619–2632, 2018.

Yijie Ding, Jijun Tang, and Fei Guo. Identification of drug-side effect association via multiple information integration with centered kernel alignment. *Neurocomputing*, 325:211–224, 2019.

Yijie Ding, Jijun Tang, and Fei Guo. Identification of drug-target interactions via multi-view graph regularized link propagation model. *Neurocomputing*, 461:618–631, 2021.

Haoyi Fan, Fengbin Zhang, Yuxuan Wei, Zuoyong Li, Changqing Zou, Yue Gao, and Qionghai Dai. Heterogeneous hypergraph variational autoencoder for link prediction. *IEEE Transactions on Pattern Analysis and Machine Intelligence*, 44(8):4125–4138, 2021.

Haitao Fu, Feng Huang, Xuan Liu, Yang Qiu, and Wen Zhang. Mvgcn: data integration through multi-view graph convolutional network for predicting links in biomedical bipartite networks. *Bioinformatics*, 38(2): 426–434, 2022.

Diego Galeano, Shantao Li, Mark Gerstein, and Alberto Paccanaro. Predicting the frequencies of drug side effects. *Nature communications*, 11(1):1–14, 2020.

Mehmet Gönen and Ethem Alpaydın. Multiple kernel learning algorithms. *The Journal of Machine Learning Research*, 12:2211–2268, 2011.

Xiaoyi Guo, Wei Zhou, Bin Shi, Xiaohua Wang, Aiyan Du, Yijie Ding, Jijun Tang, and Fei Guo. An efficient multiple kernel support vector regression model for assessing dry weight of hemodialysis patients. *Current Bioinformatics*, 16(2):284–293, 2021.

Lynn Houthuys and Johan AK Suykens. Tensor-based restricted kernel machines for multi-view classification. *Information Fusion*, 68:54–66, 2021.

Lynn Houthuys, Rocco Langone, and Johan AK Suykens. Multi-view kernel spectral clustering. *Information Fusion*, 44:46–56, 2018.

Martial Hue and Jean-Philippe Vert. On learning with kernels for unordered pairs. In *Proceedings of the 27th International Conference on Machine Learning (ICML-10)*, pp. 463–470, 2010.

Bingbing Jiang, Chenglong Zhang, Yan Zhong, Yi Liu, Yingwei Zhang, Xingyu Wu, and Weiguo Sheng. Adaptive collaborative fusion for multi-view semi-supervised classification. *Information Fusion*, 96:37–50, 2023.

Shuhui Jiang, Zhengming Ding, and Yun Fu. Heterogeneous recommendation via deep low-rank sparse collective factorization. *IEEE transactions on pattern analysis and machine intelligence*, 42(5):1097–1111, 2019.

Thomas Kailath. Rkhs approach to detection and estimation problems–i: Deterministic signals in gaussian noise. *IEEE Transactions on Information Theory*, 17(5):530–549, 1971.

Alan J Laub. *Matrix analysis for scientists and engineers*. SIAM, 2004.

Tianjiao Li, Xing-Ming Zhao, and Limin Li. Co-vae: Drug-target binding affinity prediction by co-regularized variational autoencoders. *IEEE Transactions on Pattern Analysis and Machine Intelligence*, 44(12):8861–8873, 2021.

Jiyuan Liu, Xinwang Liu, Yuexiang Yang, Qing Liao, and Yuanqing Xia. Contrastive multi-view kernel learning. *IEEE Transactions on Pattern Analysis and Machine Intelligence*, 2023.

Mei Liu, Yonghui Wu, Yukun Chen, Jingchun Sun, Zhongming Zhao, Xue-wen Chen, Michael Edwin Matheny, and Hua Xu. Large-scale prediction of adverse drug reactions using chemical, biological, and phenotypic properties of drugs. *Journal of the American Medical Informatics Association*, 19(e1):e28–e35, 2012.

Yunan Luo, Xinbin Zhao, Jingtian Zhou, Jinglin Yang, Yanqing Zhang, Wenhua Kuang, Jian Peng, Ligong Chen, and Jianyang Zeng. A network integration approach for drug-target interaction prediction and computational drug repositioning from heterogeneous information. *Nature communications*, 8(1):1–13, 2017.

Juncheng Lv, Zhao Kang, Boyu Wang, Luping Ji, and Zenglin Xu. Multi-view subspace clustering via partition fusion. *Information Sciences*, 560:410–423, 2021.

André CA Nascimento, Ricardo BC Prudêncio, and Ivan G Costa. A multiple kernel learning algorithm for drug-target interaction prediction. *BMC bioinformatics*, 17:1–16, 2016.

Jorge Nocedal and Stephen J Wright. Quadratic programming. *Numerical optimization*, pp. 448–492, 2006.

E. Pauwels, V. Stoven, and Y. Yamanishi. Predicting drug side-effect profiles: a chemical fragment-based approach. *Bmc Bioinformatics*, 12(1):169, 2011.

El.zbieta Pekalska and Bernard Haasdonk. Kernel discriminant analysis for positive definite and indefinite kernels. *IEEE transactions on pattern analysis and machine intelligence*, 31(6):1017–1032, 2008.

Michael P Perrone and Leon N Cooper. When networks disagree: Ensemble methods for hybrid neural networks. In *How We Learn; How We Remember: Toward An Understanding Of Brain And Neural Systems: Selected Papers of Leon N Cooper*, pp. 342–358. World Scientific, 1995.

Yuqing Qian, Yijie Ding, Quan Zou, and Fei Guo. Identification of drug-side effect association via restricted boltzmann machines with penalized term. *Briefings in Bioinformatics*, 23(6):bbac458, 2022a.

Yuqing Qian, Yijie Ding, Quan Zou, and Fei Guo. Multi-view kernel sparse representation for identification of membrane protein types. *IEEE/ACM Transactions on Computational Biology and Bioinformatics*, 20 (2):1234–1245, 2022b.

Rudy Raymond and Hisashi Kashima. Fast and scalable algorithms for semi-supervised link prediction on static and dynamic graphs. In *Joint european conference on machine learning and knowledge discovery in databases*, pp. 131–147. Springer, 2010.

M. Sayaka, P. Edouard, S Véronique, G. Susumu, and Y. Yoshihiro. Relating drug–protein interaction network with drug side effects. *Bioinformatics*, 2012.

S. Shabani-Mashcool, S. A. Marashi, and S. Gharaghani. Nddsa: A network- and domain-based method for predicting drug-side effect associations. *Information Processing & Management*, 57(6):102357, 2020.

Caijuan Shi, Changyu Duan, Zhibin Gu, Qi Tian, Gaoyun An, and Ruizhen Zhao. Semi-supervised feature selection analysis with structured multi-view sparse regularization. *Neurocomputing*, 330:412–424, 2019.

Jingjing Tang, Weiqi Xu, Jiahui Li, Yingjie Tian, and Shan Xu. Multi-view learning methods with the linex loss for pattern classification. *Knowledge-Based Systems*, 228:107285, 2021.

Dexian Wang, Tianrui Li, Wei Huang, Zhipeng Luo, Ping Deng, Pengfei Zhang, and Minbo Ma. A multi-view clustering algorithm based on deep semi-nmf. *Information Fusion*, pp. 101884, 2023a.

Tinghua Wang, Lin Zhang, and Wenyu Hu. Bridging deep and multiple kernel learning: A review. *Information Fusion*, 67:3–13, 2021.

Yizheng Wang, Yixiao Zhai, Yijie Ding, and Quan Zou. Sbsm-pro: Support bio-sequence machine for proteins. *arXiv preprint arXiv:2308.10275*, 2023b. doi: 10.48550/arXiv.2308.10275.

Xijiong Xie and Shiliang Sun. General multi-view semi-supervised least squares support vector machines with multi-manifold regularization. *Information Fusion*, 62:63–72, 2020.

Lixiang Xu, Lu Bai, Jin Xiao, Qi Liu, Enhong Chen, Xiaofeng Wang, and Yuanyan Tang. Multiple graph kernel learning based on gmdh-type neural network. *Information Fusion*, 66:100–110, 2021.

Xianyu Xu, Ling Yue, Bingchun Li, Ying Liu, Yuan Wang, Wenjuan Zhang, and Lin Wang. Dsgat: predicting frequencies of drug side effects by graph attention networks. *Briefings in Bioinformatics*, 23(2):bbab586, 2022.

Ping Xuan, Meng Wang, Yong Liu, Dong Wang, Tiangang Zhang, and Toshiya Nakaguchi. Integrating specific and common topologies of heterogeneous graphs and pairwise attributes for drug-related side effect prediction. *Briefings in Bioinformatics*, 23(3):bbac126, 2022.

Bo Yang, Hongbin Pei, Hechang Chen, Jiming Liu, and Shang Xia. Characterizing and discovering spatiotemporal social contact patterns for healthcare. *IEEE transactions on pattern analysis and machine intelligence*, 39(8):1532–1546, 2016.

Weiwei Yuan, Kangya He, Donghai Guan, Li Zhou, and Chenliang Li. Graph kernel based link prediction for signed social networks. *Information Fusion*, 46:1–10, 2019.

Zheng-Jun Zha, Tao Mei, Jingdong Wang, Zengfu Wang, and Xian-Sheng Hua. Graph-based semi-supervised learning with multiple labels. *Journal of Visual Communication and Image Representation*, 20(2):97–103, 2009.

Ping Zhang, Fei Wang, Jianying Hu, and Robert Sorrentino. Label propagation prediction of drug-drug interactions based on clinical side effects. *Scientific reports*, 5(1):12339, 2015.

Si Zhang, Hanghang Tong, Jiejun Xu, and Ross Maciejewski. Graph convolutional networks: a comprehensive review. *Computational Social Networks*, 6(1):1–23, 2019.

Wen Zhang, Hua Zou, Longqiang Luo, Qianchao Liu, Weijian Wu, and Wenyi Xiao. Predicting potential side effects of drugs by recommender methods and ensemble learning. *Neurocomputing*, 173:979–987, 2016.

Haochen Zhao, Kai Zheng, Yaohang Li, and Jianxin Wang. A novel graph attention model for predicting frequencies of drug–side effects from multi-view data. *Briefings in Bioinformatics*, 22(6):bbab239, 2021.

Haochen Zhao, Shaokai Wang, Kai Zheng, Qichang Zhao, Feng Zhu, and Jianxin Wang. A similarity-based deep learning approach for determining the frequencies of drug side effects. *Briefings in Bioinformatics*, 23(1):bbab449, 2022.

Yi Zou, Yijie Ding, Jijun Tang, Fei Guo, and Li Peng. Fkrr-mvsf: a fuzzy kernel ridge regression model for identifying dna-binding proteins by multi-view sequence features via chou's five-step rule. *International Journal of Molecular Sciences*, 20(17):4175, 2019.

A Appendix

A.1 Optimization

It is difficult and time-consuming to solve the Equation 24 because it contains multiple variables and large pairwise matrices. In this section, we divide the original problem into five subproblems and develop an iterative algorithm to optimize them. And, we avoid explicit computation of any pairwise matrices in the whole optimization, which makes our method suitable for solving problems in large pairwise spaces.

$\hat{\boldsymbol{F}}$-subproblem: we fix $\boldsymbol{a}^v$, $\boldsymbol{w}$, $\boldsymbol{\theta}_D$ and $\boldsymbol{\theta}_S$ to optimize variants $\hat{\boldsymbol{F}}$. Let $\boldsymbol{A} = \boldsymbol{H}_S^{-0.5}\boldsymbol{K}_S^*\boldsymbol{H}_S^{-0.5}$, $\boldsymbol{B} = \boldsymbol{H}_D^{-0.5}\boldsymbol{K}_D^*\boldsymbol{H}_D^{-0.5}$ and $\text{vec}\left(\hat{\boldsymbol{F}}^v\right) = \boldsymbol{K}^v\boldsymbol{a}^v$. Then, the optimization model of $\hat{\boldsymbol{F}}$ as follows:

$$\begin{aligned} \arg\min_{\hat{\boldsymbol{F}}} \ & \frac{1}{2}\left\|\text{vec}\left(\hat{\boldsymbol{F}}\right) - \sum_{v=1}^{V}\boldsymbol{w}_v\text{vec}\left(\hat{\boldsymbol{F}}^v\right)\right\|_2^2 + \frac{1}{2}\sigma\text{vec}\left(\hat{\boldsymbol{F}}\right)^T\boldsymbol{L}\text{vec}\left(\hat{\boldsymbol{F}}\right) \\ & s.t. \boldsymbol{L} = \boldsymbol{I}_{NM} - \boldsymbol{A}\otimes\boldsymbol{B}. \end{aligned} \tag{25}$$

Let the derivative of Equation 25 *w.r.t* $\hat{\boldsymbol{F}}$ to zero, the solution of $\hat{\boldsymbol{F}}$ can be obtained:

$$\text{vec}\left(\hat{\boldsymbol{F}}\right) = \left((1+\sigma)\,\boldsymbol{I}_{NM} - \sigma\boldsymbol{A}\otimes\boldsymbol{B}\right)^{-1}\left(\sum\nolimits_{v=1}^{V}\boldsymbol{w}_v\text{vec}\left(\hat{\boldsymbol{F}}^v\right)\right). \tag{26}$$

Notice that the inverse matrix on the right-hand side of Equation 26 needs too much time and memory. Therefore, we use eigen decomposed techniques to compute the approximate inverse. Let $\boldsymbol{V}_A\boldsymbol{\Lambda}_A\boldsymbol{V}_A^T$ and $\boldsymbol{V}_B\boldsymbol{\Lambda}_B\boldsymbol{V}_B^T$ be the eigen decomposition of the matrices $\boldsymbol{A}$ and $\boldsymbol{B}$, respectively. Define the matrix $\boldsymbol{U}$ to be $\boldsymbol{U}_{i,j} = [\boldsymbol{\Lambda}_A]_{i,i}\times[\boldsymbol{\Lambda}_B]_{j,j}$. By the theorem Raymond & Kashima (2010), the kronecker product matrix $\boldsymbol{A}\otimes\boldsymbol{B}$ can be eigendecomposed as $(\boldsymbol{V}_A\otimes\boldsymbol{V}_B)\,\text{diag}\left(\text{vec}\left(\boldsymbol{U}\right)\right)(\boldsymbol{V}_A\otimes\boldsymbol{V}_B)^T$. Then substituting it in Equation 26, we can write the inverse matrix in Equation 26 as

$$\left((1+\sigma)\,\boldsymbol{I}_{NM} - \sigma\boldsymbol{A}\otimes\boldsymbol{B}\right)^{-1} = \left((1+\sigma)\,\boldsymbol{I}_{NM} - \sigma(\boldsymbol{V}_A\otimes\boldsymbol{V}_B)\,\text{diag}\left(\text{vec}\left(\boldsymbol{U}\right)\right)(\boldsymbol{V}_A\otimes\boldsymbol{V}_B)^T\right)^{-1}. \tag{27}$$

Since, it holds that $(\boldsymbol{V}_A\otimes\boldsymbol{V}_B)(\boldsymbol{V}_A\otimes\boldsymbol{V}_B)^T = \boldsymbol{I}_{NM}$. Equation 27 can be transformed into

$$\left((1+\sigma)\,\boldsymbol{I}_{NM} - \sigma\boldsymbol{A}\otimes\boldsymbol{B}\right)^{-1} = (\boldsymbol{V}_A\otimes\boldsymbol{V}_B)\left((1+\sigma)\,\boldsymbol{I}_{NM} - \sigma\text{diag}\left(\text{vec}\left(\boldsymbol{U}\right)\right)\right)^{-1}(\boldsymbol{V}_A\otimes\boldsymbol{V}_B)^T. \tag{28}$$

Notice that the inverse matrix in Equation 28 is a diagonal matrix whose value can be calculated as the matrix $\boldsymbol{W}$

$$\boldsymbol{W}_{i,j} = (1+\sigma-\sigma\boldsymbol{U}_{i,j})^{-1} \tag{29}$$

So, we can further rewrite the Equation 26 as

$$\text{vec}\left(\hat{\boldsymbol{F}}\right) = (\boldsymbol{V}_A\otimes\boldsymbol{V}_B)\text{diag}\left(\text{vec}\left(\boldsymbol{W}\right)\right)(\boldsymbol{V}_A\otimes\boldsymbol{V}_B)^T\left(\sum\nolimits_{v=1}^{V}\boldsymbol{w}_v\text{vec}\left(\hat{\boldsymbol{F}}^v\right)\right) \tag{30}$$

Taking out the vec-tricks operation, we can obtain the solution

$$\hat{\boldsymbol{F}} = \boldsymbol{V}_B\left(\boldsymbol{W}\odot\left(\boldsymbol{V}_B^T\left(\sum\nolimits_{v=1}^{V}\boldsymbol{w}_v\hat{\boldsymbol{F}}^v\right)\boldsymbol{V}_A\right)\right)\boldsymbol{V}_A^T \tag{31}$$

$\boldsymbol{w}$-subproblem: we fix all the variants except $\boldsymbol{w}$. The formula is as follows:

$$\begin{aligned} \arg\min_{\boldsymbol{w}} \ & \frac{1}{2}\left\|\hat{\boldsymbol{F}} - \sum_{v=1}^{V}\boldsymbol{w}_v\hat{\boldsymbol{F}}^v\right\|_F^2 + \mu\sum_{v=1}^{V}\left(\frac{\boldsymbol{w}_v}{2}\left\|\boldsymbol{F} - \hat{\boldsymbol{F}}^v\right\|_F^2\right) + \frac{1}{2}\beta\left\|\boldsymbol{w}\right\|_2^2 \\ & s.t. \sum_{v=1}^{V}\boldsymbol{w}_v = 1, \boldsymbol{w}_v \geq 0, v = 1,\ldots,V. \end{aligned} \tag{32}$$

Problem 32 can be simplified as a standard quadratic programming problem Nocedal & Wright (2006)

$$\begin{aligned} \arg\min_{\boldsymbol{w}} \ & \boldsymbol{w}^T\boldsymbol{G}\boldsymbol{w} - \boldsymbol{w}^T\boldsymbol{h} \\ & s.t. \sum_{v=1}^{V}\boldsymbol{w}_v = 1, \boldsymbol{w}_v \geq 0, v = 1,\ldots,V. \end{aligned} \tag{33}$$

where $\boldsymbol{G} \in \mathbb{R}^{V \times V}$ with the element as

$$\boldsymbol{G}_{i,j} = \begin{cases} \frac{1}{2}\text{trace}\left(\left(\hat{\boldsymbol{F}}^i\right)^T \hat{\boldsymbol{F}}^j\right), & \text{if } i \neq j, \\ \frac{1}{2}\text{trace}\left(\left(\hat{\boldsymbol{F}}^i\right)^T \hat{\boldsymbol{F}}^j\right) + \frac{1}{2}\beta, & \text{if } i = j. \end{cases} \tag{34}$$

$\boldsymbol{h}$ is a vector with

$$\boldsymbol{h}_i = \text{trace}\left(\hat{\boldsymbol{F}}^T \hat{\boldsymbol{F}}^i\right) - \frac{\mu}{2}\left\|\boldsymbol{F} - \hat{\boldsymbol{F}}^i\right\|_F^2. \tag{35}$$

The optimization method for Equation 33 is the interior-point optimization algorithm Byrd et al. (1999).

$\boldsymbol{\theta}_D$-subproblem: With the fixed all the variants except $\boldsymbol{\theta}_D$, the formula can be written as

$$\begin{aligned} \arg\min_{\boldsymbol{\theta}_D} \ & \frac{1}{2}\sigma\text{vec}\left(\hat{\boldsymbol{F}}\right)^T \boldsymbol{L}\text{vec}\left(\hat{\boldsymbol{F}}\right) \\ s.t.\ & \boldsymbol{L} = \boldsymbol{I}_{NM} - \left(\boldsymbol{H}_S^{-0.5}\boldsymbol{K}_S^*\boldsymbol{H}_S^{-0.5}\right) \otimes \left(\boldsymbol{H}_D^{-0.5}\boldsymbol{K}_D^*\boldsymbol{H}_D^{-0.5}\right), \\ & \boldsymbol{K}_D^* = \sum_{i=1}^{P} [\boldsymbol{\theta}_D]_i^{\varepsilon} \boldsymbol{K}_D^i, \sum_{i=1}^{P} [\boldsymbol{\theta}_D]_i = 1, [\boldsymbol{\theta}_D]_i \geq 0, i = 1, \ldots, P. \end{aligned} \tag{36}$$

Let $\boldsymbol{A} = \boldsymbol{H}_S^{-0.5}\boldsymbol{K}_S^*\boldsymbol{H}_S^{-0.5}$ and $\boldsymbol{B}^i = \boldsymbol{H}_D^{-0.5}\boldsymbol{K}_D^i\boldsymbol{H}_D^{-0.5}$. Then substituting $\boldsymbol{L}$ in Equation 36 with $\boldsymbol{A}$ and $\boldsymbol{B}^i$, the objective function 36 can be written as

$$\begin{aligned} \arg\min_{\boldsymbol{\theta}_D} \ & -\frac{1}{2}\sigma\text{vec}\left(\hat{\boldsymbol{F}}\right)^T \sum_{i=1}^{P} \left(\boldsymbol{A} \otimes \boldsymbol{B}^i\right)\text{vec}\left(\hat{\boldsymbol{F}}\right) \\ & s.t. \sum_{i=1}^{P} [\boldsymbol{\theta}_D]_i = 1, [\boldsymbol{\theta}_D]_i \geq 0, i = 1, \ldots, P. \end{aligned} \tag{37}$$

Further, introduce the Lagrange multiplier ξ and the objective function 37 can be converted to a Lagrange function:

$$\text{Lag}\left(\boldsymbol{\theta}_D, \xi\right) = -\frac{1}{2}\sigma\text{vec}\left(\hat{\boldsymbol{F}}\right)^T \sum_{i=1}^{P} \left(\boldsymbol{A} \otimes \boldsymbol{B}^i\right)\text{vec}\left(\hat{\boldsymbol{F}}\right) - \xi\left(\sum_{i=1}^{P} [\boldsymbol{\theta}_D]_i - 1\right) \tag{38}$$

Based on setting the derivative of Equation 38 *w.r.t* $\boldsymbol{\theta}_D$ and ξ to zero respectively, we have the following solution

$$[\boldsymbol{\theta}_D]_i = \left(\text{vec}\left(\hat{\boldsymbol{F}}\right)^T \left(\boldsymbol{A} \otimes \boldsymbol{B}^i\right)\text{vec}\left(\hat{\boldsymbol{F}}\right)\right)^{\frac{1}{1-\varepsilon}} \Bigg/ \sum_{j=1}^{P} \left(\text{vec}\left(\hat{\boldsymbol{F}}\right)^T \left(\boldsymbol{A} \otimes \boldsymbol{B}^j\right)\text{vec}\left(\hat{\boldsymbol{F}}\right)\right)^{\frac{1}{1-\varepsilon}}. \tag{39}$$

By using the vec-tricks operation, we can describe the solution as

$$[\boldsymbol{\theta}_D]_i = \text{trace}\left(\hat{\boldsymbol{F}}^T \boldsymbol{B}^i \hat{\boldsymbol{F}} \boldsymbol{A}^T\right)^{\frac{1}{1-\varepsilon}} \Bigg/ \sum_{j=1}^{P} \text{trace}\left(\hat{\boldsymbol{F}}^T \boldsymbol{B}^j \hat{\boldsymbol{F}} \boldsymbol{A}^T\right)^{\frac{1}{1-\varepsilon}} \tag{40}$$

$\boldsymbol{\theta}_S$-subproblem:The solution of $\boldsymbol{\theta}_S$ is similarity to $\boldsymbol{\theta}_D$. Here, the optimization process is omitted and we directly give the solution

$$[\boldsymbol{\theta}_S]_i = \text{trace}\left(\hat{\boldsymbol{F}}^T \boldsymbol{B} \hat{\boldsymbol{F}} (\boldsymbol{A}^i)^T\right)^{\frac{1}{1-\varepsilon}} \Bigg/ \sum_{j=1}^{Q} \text{trace}\left(\hat{\boldsymbol{F}}^T \boldsymbol{B} \hat{\boldsymbol{F}} (\boldsymbol{A}^j)^T\right)^{\frac{1}{1-\varepsilon}} \tag{41}$$

where $\boldsymbol{B} = \boldsymbol{H}_D^{-0.5}\boldsymbol{K}_D^*\boldsymbol{H}_D^{-0.5}$ and $\boldsymbol{A}^i = \boldsymbol{H}_S^{-0.5}\boldsymbol{K}_S^i\boldsymbol{H}_S^{-0.5}$.

a^v-subproblem: By dropping all other irrelevant terms with respect $\boldsymbol{a}^v$, we have

$$\arg\min_{\boldsymbol{a}^v} \frac{1}{2}\left\|\text{vec}\left(\hat{\boldsymbol{F}}\right) - \sum_{i=1}^{V} \boldsymbol{w}_i \boldsymbol{K}^i \boldsymbol{a}^i\right\|_2^2 + \mu\left(\frac{\boldsymbol{w}_v}{2}\left\|\text{vec}\left(\boldsymbol{F}\right) - \boldsymbol{K}^v\boldsymbol{a}^v\right\|_2^2 + \frac{\lambda^v}{2}{\boldsymbol{a}^v}^T\boldsymbol{K}^v\boldsymbol{a}^v\right). \tag{42}$$

It can be observed from the objective function 42 that when training the parameter $\boldsymbol{a}^v$, other views $\boldsymbol{K}_i$ with weight $\boldsymbol{w}_i$ were taken into consideration. Therefore, each partition's training is not completely separate, but involves information sharing.

Based on setting the derivative of problem 42 *w.r.t* $\boldsymbol{a}^v$ to zero, we get

$$\left(\boldsymbol{K}^v + \frac{\lambda_v}{1+\mu\boldsymbol{w}_v}\boldsymbol{I}_{NM}\right)\boldsymbol{a}^v = \frac{1}{1+\mu\boldsymbol{w}_v}\left(\text{vec}\left(\hat{\boldsymbol{F}}\right) - \sum_{i=1,i\neq v}^{V}\boldsymbol{w}_i\boldsymbol{K}^i\boldsymbol{a}^i + \mu\boldsymbol{w}_v\text{vec}\left(\boldsymbol{F}\right)\right) \tag{43}$$

Let $\boldsymbol{W} = \hat{\boldsymbol{F}} - \sum_{i=1,i\neq v}^{V}\boldsymbol{w}_i\hat{\boldsymbol{F}}^i + \mu\boldsymbol{w}_v\boldsymbol{F}$, the Equation 43 can be written as

$$\boldsymbol{a}^v = \frac{1}{1+\mu\boldsymbol{w}_v}\left(\boldsymbol{K}^v + \frac{\lambda_v}{1+\mu\boldsymbol{w}_v}\boldsymbol{I}_{NM}\right)^{-1}\text{vec}\left(\boldsymbol{W}\right). \tag{44}$$

We can observe that the form of Equation 44 is similar to Equation 7. Therefore, we use eigen decomposed techniques and the vec-trick operation to effectively compute $\boldsymbol{a}^v$.

We summarize the complete optimization process for problem 24 in Algorithm 1.

Algorithm 1: Optimization for MKronRLSF-LP.

Input: The link matrix $\boldsymbol{F}$; The regulation parameters μ, β, σ, ε and $\lambda^v, v = 1, \ldots, V$;
Output: The predicted link matrix $\hat{\boldsymbol{F}}$;

```
Compute two sets of base kernel sets 𝕂_D and 𝕂_S by Equation 20a and 20b;
Initialize a^v, v = 1,...,V by single view Kron-RLS; w_v = 1/V, v = 1,...,V; θ_D^i = 1/P, i = 1,...,P;
  θ_S^i = 1/Q, i = 1,...,Q;
while Not convergence do
    Update F̂ by solve the subproblem 25;
    Update w by solve the subproblem 32;
    Update θ_D by solve the subproblem 36;
    Update θ_S by Equation 41;
    for i = 1 to V do
        Update a^i by solve the subproblem 42;
    end
end
```

A.2 Evaluation Metric

Considering that drug-side effect prediction is an extremely imbalanced classification problem and we do not want incorrect predictions to be recommended by the prediction model, we utilize the following evaluation parameters:

$$Recall = \frac{TP}{TP+FN}, \tag{45a}$$

$$Precision = \frac{TP}{TP+FP}, \tag{45b}$$

$$F_{score} = 2 \times \frac{Precision \times Recall}{Precision + Recall}, \tag{45c}$$

where TP, FN, FP and TN are the number of true-positive samples, false-negative samples, false-positive samples and true-negative samples, respectively. The area under the ROC curve (AUC) and area under the precision recall curve (AUPR) is also used to measure predictive accuracy, because they are the most commonly used evaluate metrics in the biomedical link prediction. Notice that AUPR heavily penalizes non-links that are highly ranked, which is desirable here.

A.3 Baseline methods

- Best single view (BSV): Applying Kron-RLS to the best single view. The one with the maximum AUPR is chosen here.
- Committee Kron-RLS (Comm Kron-RLS)Perrone & Cooper (1995): Each view is trained by Kron-RLS separately, and the final classifier is a weighted average.
- Kron-RLS with Centered Kernel Alignment-based Multiple Kernel Learning (Kron-RLS+CKA-MKL)Ding et al. (2019): Multiple kernels from the drug space and side effect space are linearly weighted by the optimized CKA-MKL. Finally, Kron-RLS is employed on optimal kernels.
- Kron-RLS with pairwise Multiple Kernel Learning (Kron-RLS+pairwiseMKL)Cichonska et al. (2018): First, it constructs multiple pairwise kernels. Then, the mixture weights of the pairwise kernels are determined by CKA-MKL. Finally, it learns the Kron-RLS function based on the optimal pairwise kernel.
- Kron-RLS with self-weighted multiple kernel learning (Kron-RLS+self-MKL)Nascimento et al. (2016): The optimal drug and side effect kernels are linearly weighted based on the multiple base kernel. The proper weights assignment to each kernel is performed automatically.
- Multi-view graph regularized link propagation model (MvGRLP)Ding et al. (2021): This is an extension of the graph model Zha et al. (2009). To fuse multi view information, multi-view Laplacian regularization is introduced to constrain the predicted values.
- Multi-view graph convolution network (MVGCN)Fu et al. (2022): This extends the GCN Zhang et al. (2019) from a single view to multi-view by combining the embeddings of multiple neighborhood information aggregation layers in each view.

A.4 Code and Data Available

The code and data are available at `https://figshare.com/articles/dataset/MKronRLSF-LP/24203661`.

A.5 Tables of Parameter Setting

Table 7: The optimal parameters λ^v obtained with the single view Kron-RLS model (based on the relative pairwise kernel).

$\otimes$	$\boldsymbol{K}_{GIP,S}$	$\boldsymbol{K}_{GIP,S}$	$\boldsymbol{K}_{GIP,S}$	$\boldsymbol{K}_{GIP,S}$	$\boldsymbol{K}_{GIP,S}$
$\boldsymbol{K}_{GIP,D}$	2^0	2^2	2^2	2^1	2^1
$\boldsymbol{K}_{COS,D}$	2^2	2^3	2^3	2^2	2^{-2}
$\boldsymbol{K}_{Corr,D}$	2^3	2^3	2^4	2^2	2^4
$\boldsymbol{K}_{MI,D}$	2^0	2^1	2^1	2^0	2^{-1}
$\boldsymbol{K}_{NTK,D}$	2^2	2^4	2^3	2^1	2^1

Table 8: Summary of the threshold of baseline methods on four datasets.

Methods	Liu	Pau	Miz	Luo
BSV	0.145	0.146	0.142	0.128
Comm Kron-RLS	0.205	0.204	0.192	0.183
Kron-RLS+CKA-MKL	0.100	0.106	0.099	0.102
Kron-RLS+pairwiseMKL	0.149	0.159	0.101	0.107
Kron-RLS+self-MKL	0.119	0.116	0.113	0.129
MvGRLP	0.090	0.091	0.094	0.085
MVGCN	0.225	0.237	0.208	0.197
MKronRLSF-LP	0.177	0.168	0.179	0.149